

Part-aware Shape Generation with Latent 3D Diffusion of Neural Voxel Fields

Yuhang Huang, Shilong Zou, Xinwang Liu, and Kai Xu*

National University of Defense Technology, China

Abstract. This paper presents a novel latent 3D diffusion model for the generation of neural voxel fields, aiming to achieve accurate part-aware structures. Compared to existing methods, there are two key designs to ensure high-quality and accurate part-aware generation. On one hand, we introduce a latent 3D diffusion process for neural voxel fields, enabling generation at significantly higher resolutions that can accurately capture rich textural and geometric details. On the other hand, a part-aware shape decoder is introduced to integrate the part codes into the neural voxel fields, guiding the accurate part decomposition and producing high-quality rendering results. Through extensive experimentation and comparisons with state-of-the-art methods, we evaluate our approach across four different classes of data. The results demonstrate the superior generative capabilities of our proposed method in part-aware shape generation, outperforming existing state-of-the-art methods.

Keywords: Shape Generation · Diffusion Model · Part-aware Generation

1 Introduction

Recent generative models have emerged for generating 3D shapes with different representations [10, 14, 37, 44], among which neural field representation [3, 4, 12, 27, 33, 46] receives increasing attention due to many advantages such as integrated texture and shape generation. Despite the fast and notable progress made along this line of research, what has been largely missed is part/structure awareness. Most existing generative models based on neural fields are part-oblivious. They tend to generate 3D shapes in a holistic manner, without comprehending its compositional parts explicitly.

Generating 3D shapes with part information facilitates several downstream processing/tasks, such as editing, mix-and-match modeling, and segmentation learning. SPAGHETTI [15] and Part-NeRF [42] are two excellent part-aware generative models for 3D shape synthesis with neural field representation. Despite their strengths, there is still potential for enhancing the generative ability. SPAGHETTI relies on 3D supervision and mainly consider the geometry, ignoring the textured shape generation. On the other hand, Part-NeRF requires only

* corresponding author.

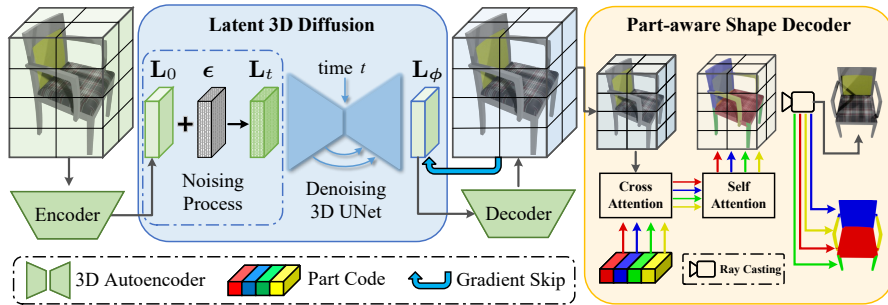


Fig. 1: The proposed method comprises two main modules: a latent 3D diffusion model and a part-aware shape decoder. The latent 3D diffusion model facilitates high-resolution generation of neural voxel fields, while the part-aware shape decoder enables the generation of parts-aware results for rendering. The two modules are trained in an end-to-end fashion.

2D supervision but adopts a complex architecture with multiple neural radiance fields, leading to increased complexity in learning and subpar rendering outcomes. Moreover, both models perform object segmentation in an unsupervised manner, resulting in structurally insignificant information.

We propose a latent 3D diffusion model to generate neural voxel fields with accurate structural details in this paper. As shown in Fig 1, our network is composed of two parts, a latent 3D diffusion model of neural voxel fields and a part-aware shape decoder. Specifically, the latent 3D diffusion model utilizes the advantage of 3D convolution and employs the 3D denoising process in a latent space with much lower resolution. On the other hand, the part-aware shape decoder incorporates the part code with the neural voxel field, guiding the precise generation of part-aware shapes and synthesizing high-quality rendering results.

Benefiting from the latent diffusion design, our model allows for shape generation with a much higher resolution than previous work (e.g., Matthias [24]). In particular, our method achieves 96^3 resolution which is sufficient for representing rich geometric details of most common-seen objects. Furthermore, we integrate cross- and self-attention mechanisms into the part-aware decoder to establish robust dependencies between the part code and the voxel field. This integration aids in modeling the inherent relationships among various parts, significantly enhancing the precision of part segmentation.

Our method adopts full volume learning part-learning and decoder-based part decomposition. This avoids the design of per-part neural fields which makes the decomposition and rendering overly complicated. Our architecture makes rendering rather simplistic and allows for high-quality rendering and hence accurate training.

The diffusion model admits multi-modal prompt for shape generation. For example, we have implemented image-conditioned diffusion enabling single-image

guided generation. Concretely, a convolutional encoder is employed to extract features from the reference image. Subsequently, these obtained features are combined with the multi-scale features of the denoising UNet. As a result, the image information can effectively guide the shape generation.

To make a fair comparison, we have implemented a supervised version of Part-NeRF. Similar to acquiring color, we use MLP layers to implicitly learn the part emission of 3D position, obtaining the semantic part map via volume rendering. We conduct extensive experiments and compare to the state-of-the-art methods on four classes of common-seen objects. The results show that our method achieves the best FID metric on all classes of data and higher-quality part-aware generation.

2 Related Work

GANs for Shape Generation. Recent developments in generative models have enabled the synthesis of 3D shapes through a variety of representations, including point clouds [1,35], voxels [14,25,26], meshes [10], and neural fields [4,7,20,34,38]. In particular, the neural field representation has demonstrated significant potential as it enables photo-realistic renderings of 3D objects and can be trained with only 2D image supervision. With the success of Generative Adversarial Network (GAN) [11] in 2D vision, most studies apply it to neural field generation. PiGAN [4] and GRAF [33] propose to generate neural fields with stochastic latent codes, and the following GIRAFFE [27] represents the scene as the compositional neural feature field with a similar way. StyleNeRF [12] attempts to increase the generative consistency via the new upsampler and regularization loss. Furthermore, EG3D [3] proposes to use a convolutional network to generate neural tri-plane fields, improving the training efficiency. Different from these methods, we aim to generate part-aware neural voxel field with diffusion models.

Diffusion Models for Generating Neural Fields. Recently, the diffusion models [16,39] has outperformed GANs in various of 2D tasks [8], which inspires several diffusion-based methods to generate neural fields. DreamFusion [29] utilizes the 2D pretrained diffusion model as the distillation model to guide the generation of neural fields for the first time. Following this idea, a series of researches [22,30,47] can edit and generate neural fields via text prompt. However, they need to retrain the model for each generation, leading to a time-consuming generating process. Differently, another line of work directly apply the diffusion model to synthesize the neural fields without 2D pretrained diffusion model. DiffRF [24] applies the diffusion model to generate neural voxel fields, however, the 3D convolutional network takes up too much memory cost, limiting the generated resolution. SSD-NeRF [31] proposes a single-stage training paradigm to generate tri-plane fields with 2D convolutional network. In this paper, we propose a 3D latent diffusion model to directly generate neural voxel fields, enabling high-resolution and high-quality generation.

Part-aware Shape Generation. Previous methods [13,15,19,28,45] usually generate part-aware shapes with point cloud representation, however, they

usually use the 3D supervision. Recent PartNeRF [42] proposes to represent the different parts of a shape with different neural radiance fields, however, the divided parts are meaningless and multiple neural fields require much high computational resources. Differently, we carefully design the part relation module and supervise the model with 2D part mask, achieving precise and high-quality part-aware shape generation.

3 Proposed Method

In this section, we introduce a latent 3D diffusion model to generate high-resolution part-aware neural voxel fields. As illustrated in Fig. 1, our approach consists of a latent 3D diffusion model and a part-aware shape decoder. Specifically, the latent 3D diffusion model compresses the object fields into the latent space with much smaller spacial resolution, and then adopts the 3D Unet to conduct the diffusion process. This implementation facilitates the high resolution of the voxel field, allowing the high-quality rendering results. On the other hand, the part-aware shape decoder integrates the part codes into the voxel field, establishing relationships between different parts of the voxel field, and produces RGB images and semantic part maps through ray casting.

3.1 Preliminary

Neural Voxel Fields Neural radiance fields (NeRFs) [23] represent 3D object implicitly and map the 3D position \mathbf{x} and view direction \mathbf{d} to the density σ and color emission \mathbf{c} , obtaining the novel view image via volume rendering. Based on NeRFs, DVGO [41] learns neural voxel fields to represent the object density and color. Specifically, there are a density voxel field and a feature voxel field, which are represented by \mathbf{V}^σ and \mathbf{V}^c . We can acquire the the density and color feature of position \mathbf{x} by querying from \mathbf{V}^σ and \mathbf{V}^c directly, and the color feature and view direction are feed into multilayer perceptron (MLP) layers to get the color emission \mathbf{c} .

$$\begin{aligned} \text{query}(\mathbf{V}, \mathbf{x}) &: (\mathbb{R}^{C \times X \times Y \times Z}, \mathbb{R}^3) \rightarrow \mathbb{R}^C, \\ \sigma &= \text{query}(\mathbf{V}^\sigma, \mathbf{x}), \\ \mathbf{c} &= \text{MLP}(\text{query}(\mathbf{V}^c, \mathbf{x}); \mathbf{d}). \end{aligned} \tag{1}$$

Here, $\text{query}(\mathbf{V}, \mathbf{x})$ denotes the function querying the value of position \mathbf{x} from the voxel field \mathbf{V} , C is the dimension of the modality, and (X, Y, Z) is the spatial size of \mathbf{V} . With the ray casting, the RGB color of a given ray \mathbf{r} can be rendered by the following equation:

$$\begin{aligned} \hat{\mathbf{c}}(\mathbf{r}) &= \sum_{i=1}^M \left(\prod_{j=1}^{i-1} (1 - \alpha_j) \right) \alpha_i \mathbf{c}_i, \\ \alpha_i &= 1 - \exp(-\sigma_i \delta_i), \end{aligned} \tag{2}$$

where M is the number of sampled points along the ray, α_i is the probability of the termination at point i , δ_i is the distance between the sampled point and its

adjacent point. In this way, the neural voxel field can be optimized by minimizing the mean square error of the rendered RGB $\hat{\mathbf{c}}(\mathbf{r})$ and the ground truth color $\mathbf{g}_c(\mathbf{r})$. After the optimization, we can represent the object with \mathbf{V}^σ and \mathbf{V}^c . To simply formulation, we concatenate \mathbf{V}^σ and \mathbf{V}^c along the first dimension, resulting in \mathbf{V}^f as representation of the neural voxel field.

Decoupled Diffusion Models Diffusion models has shown the great potential in generative tasks, however, it usually suffers from prolonged inference time. Recent decoupled diffusion models [17] propose to decouple the diffusion process to speed up the sampling process. The decoupled forward diffusion process is controlled by the analytic data attenuation and the standard Wiener process:

$$q(\mathbf{V}_t^f | \mathbf{V}_0^f) = \mathcal{N}(\mathbf{V}_0^f + \int_0^t \mathbf{a}_t dt, t\mathbf{I}), \quad (3)$$

where $t \in [0, 1]$ is the time step, $\mathbf{V}_0^f = \mathbf{V}^f$ is the original voxel field and \mathbf{V}_t^f is the noisy field at time t . \mathbf{a}_t is the analytic attenuation function describing the process of the original voxel field to zero field, and \mathbf{I} is the identity matrix. According to the derivation of [17], the corresponding reversed process is written as:

$$q(\mathbf{V}_{t-\Delta t}^f | \mathbf{V}_t^f, \mathbf{V}_0^f) = \mathcal{N}(\mathbf{V}_t^f - \int_{t-\Delta t}^t \mathbf{a}_t dt - \frac{\Delta t}{\sqrt{t}} \boldsymbol{\epsilon}, \frac{\Delta t(t - \Delta t)}{t} \mathbf{I}), \quad (4)$$

where Δt is the time interval, $\boldsymbol{\epsilon} \sim \mathcal{N}(\mathbf{0}, \mathbf{I})$ is the standard normal noise. Benefiting from the analytic attenuation function, we can solve the reversed process with arbitrary time interval via analytic integration, improving the sampling efficiency greatly. In practice, we choose the particular constant form of \mathbf{a}_t : $\mathbf{a}_t = -\mathbf{V}_0^f$. In this way, the model is supervised by $\boldsymbol{\epsilon}$ and \mathbf{V}_0^f simultaneously, and the training objective is formulated by:

$$\min_{\boldsymbol{\theta}} \mathbb{E}_{q(\mathbf{V}_0^f)} \mathbb{E}_{q(\boldsymbol{\epsilon})} [\|\mathbf{a}_{\boldsymbol{\theta}} + \mathbf{V}_0^f\|^2 + \|\boldsymbol{\epsilon}_{\boldsymbol{\theta}} - \boldsymbol{\epsilon}\|^2], \quad (5)$$

where $\boldsymbol{\theta}$, $\mathbf{a}_{\boldsymbol{\theta}}$ and $\boldsymbol{\epsilon}_{\boldsymbol{\theta}}$ are the parameter and two outputs of the diffusion model respectively.

3.2 Latent 3D Diffusion Model

Inspired by the preliminary work, we introduce a latent 3D diffusion model for the generation of high-resolution neural voxel fields. Our model offers two key advantages in comparison to previous diffusion-based methods. Unlike conventional 2D diffusion models [8, 16, 32, 40], we utilize 3D convolution to directly denoise the voxel field in 3D space, which enhances our modeling capabilities in terms of 3D geometry and consistency. On the other hand, due to the substantial computational demands of 3D convolution, training a 3D diffusion model with high-resolution voxel fields proves challenging, thereby constraining the generative quality. To address this limitation, we shift the denoising process to a latent

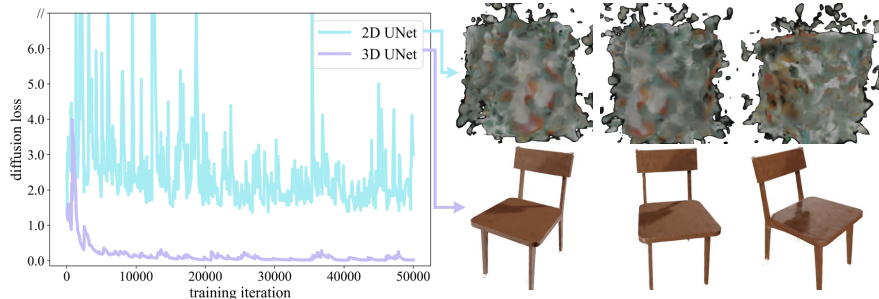


Fig. 2: Comparison between different denoising networks. The left sub-figure depicts the training curves of 2D UNet and 3D UNet, while the right sub-figure shows the visual results of their generations.

space with reduced resolution, effectively eliminating constraints on voxel field resolution.

As shown in Fig. 1, the proposed latent 3D diffusion model comprises a 3D autoencoder and a 3D denoising UNet. The 3D autoencoder has an encoder for compressing the voxel field \mathbf{V}_0^f to the latent code \mathbf{L}_0 and a decoder for recovering the original voxel field from \mathbf{L}_0 , i.e. $\mathbf{L}_0 = \mathcal{E}(\mathbf{V}_0^f)$, $\hat{\mathbf{V}}_0^f = \mathcal{D}(\mathbf{L}_0)$. Here, \mathcal{E} and \mathcal{D} represent the encoder and decoder of the 3D autoencoder; $\hat{\mathbf{V}}_0^f$ is the reconstructed voxel field. In practice, the resolution of \mathbf{L}_0 is $64\times$ lower than \mathbf{V}_0^f . After obtaining the latent code, we adopt a 3D Unet architecture to conduct the diffusion process in the latent space. Similar to Eq. 3, we sample the noisy code \mathbf{L}_t by adding the normal noise ϵ to \mathbf{L}_0 . Then, the noisy code is fed into the 3D UNet with the time t together, outputting the estimations of \mathbf{L}_0 and ϵ . This process is formulated by:

$$\begin{aligned} \mathbf{L}_t &= (1 - t)\mathbf{L}_0 + \sqrt{t}\epsilon, \\ \mathbf{L}_\phi, \epsilon_\phi &= \text{UNet}_\phi(\mathbf{L}_t, t), \end{aligned} \quad (6)$$

where ϕ is the parameter of 3D UNet, \mathbf{L}_ϕ and ϵ_ϕ are the predictions of \mathbf{L}_0 and ϵ . Note that we use the special form of the attenuation function: $\mathbf{a}_t = -\mathbf{L}_0$.

3D Unet vs. 2D UNet. Actually, though the latent code \mathbf{L}_t is a 4D tensor, it is possible to apply the 2D convolutional operator to this type of data. In practice, we can reshape \mathbf{L}_t into a 3D tensor, i.e. $\text{reshape}(\mathbb{R}^{C\times X\times Y\times Z}) \rightarrow \mathbb{R}^{C\times X\times Y\times Z}$, thus adopting 2D UNet to model the denoising process. However, we found that it failed to obtain satisfactory results as shown in Fig. 2. We assume that the 2D UNet architecture hardly learns the 3D consistency of the voxel field, resulting in a perturbed result. In contrast, the 3D UNet architecture provides reasonable performance, demonstrating the necessity of adopting 3D UNet for denoising the neural voxel field.

3.3 Part-aware Shape Decoder

After the denoising process of the latent 3D diffusion model, we can have a neural voxel field containing the density and color feature. However, it can not provide the structural information and rendering results. Therefore, we propose a part-aware shape decoder to generate part-aware details and rendering results.

As shown in Fig. 1, to model the part-aware information, the shape decoder integrates the part code into the voxel field and utilize the part attention to build the relations between different parts of the voxel field. Specifically, the part code is a learnable embedding and can be represented by $\mathbf{z} \in \mathbb{R}^{K \times D}$, where K is the number of parts, D is the dimension of the embedding. To incorporate the part code into the neural field, we first project the reconstructed voxel field $\hat{\mathbf{V}}_0^f$ to have the same dimension as \mathbf{z} , and then flatten $\hat{\mathbf{V}}_0^f$ to be a 2D tensor like $\mathbb{R}^{XYZ \times D}$. Thus, we can utilize the multi-head cross-attention [43] to build strong dependency between the part code and the voxel field. Moreover, to divide the voxel field accurately, we employ a self-attention to model the long-range relations between the different parts of the voxel field. After the cross-attention and self-attention, we reshape the tensor back to be a 4D voxel field. We formulate this process by the following equation:

$$\bar{\mathbf{V}}_0^f = \text{MHSA}(\text{MHCA}(\mathbf{z}, \hat{\mathbf{V}}_0^f)), \bar{\mathbf{V}}_0^f \in \mathbb{R}^{D \times X \times Y \times Z}, \quad (7)$$

where MHSA and MHCA represents the multi-head self-attention and cross-attention.

Incorporated with the part code, the refined voxel field $\bar{\mathbf{V}}_0^f$ contains both the color and structural information. In this way, we can utilize the volume rendering to generate images and part maps of arbitrary views. Given a 3D position \mathbf{x} , we can query the point feature of the voxel field, and acquire the color and part emissions with MLP layers.

$$\begin{aligned} \mathbf{c} &= \text{MLP}(\text{query}(\bar{\mathbf{V}}_0^f, \mathbf{x}); \mathbf{d}; \mathbf{z}), \\ \mathbf{p} &= \text{MLP}(\text{query}(\bar{\mathbf{V}}_0^f, \mathbf{x}); \mathbf{z}), \end{aligned} \quad (8)$$

where $\mathbf{p} \in \mathbb{R}^K$ is the part emission. In contrast to Eq. 3, we incorporate the part code into the MLP layers collectively to encode the structural information into individual points, thereby enhancing the generative intricacies. Subsequently, we derive the RGB image and semantic part map via ray casting following Eq. 2.

3.4 End-to-end Training with Gradient Skip

Several methods [2, 9] in the literature have combined the diffusion model with the neural field decoder, typically training these two components independently. However, independent training neglects the consideration of noise in the prior term $\hat{\mathbf{V}}_0^f$ during the training of the neural field decoder, leading to biased learning of the decoder. In contrast, we propose an end-to-end training approach for the

latent 3D diffusion model and the part-aware shape decoder, thereby avoiding noisy generation.

Gradient Skip. The diffusion model is trained on the latent space while the part-aware shape decoder is applied to the voxel field directly. Besides, there is the decoder \mathcal{D} of the 3D autoencoder between the two modules connecting the latent space and the voxel field space. Obviously, training the two modules jointly needs the backward propagation of the gradient of \mathcal{D} . However, this implementation incurs significant computational costs and hinders the effective feedback of gradients. To mitigate this problem, we propose to skip the gradient of \mathcal{D} , allowing the gradient of the part-aware shape decoder to directly propagate back to the latent space. Concretely, according to the Chain Rule, we have:

$$\nabla_{\phi} \mathcal{L}_{rend} = \frac{\partial \mathcal{L}_{rend}}{\partial \hat{\mathbf{V}}_0^f} \frac{\partial \hat{\mathbf{V}}_0^f}{\partial \mathbf{L}_{\phi}} \frac{\partial \mathbf{L}_{\phi}}{\partial \phi}, \quad (9)$$

where \mathcal{L}_{rend} is the rendering loss. We ignore the term $\partial \hat{\mathbf{V}}_0^f / \partial \mathbf{L}_{\phi}$ to skip the gradient of decoder in the 3D autoencoder, resulting in a efficient formulation of gradient calculation:

$$\nabla_{\phi} \mathcal{L}_{rend} = \frac{\partial \mathcal{L}_{rend}}{\partial \hat{\mathbf{V}}_0^f} \frac{\partial \mathbf{L}_{\phi}}{\partial \phi}. \quad (10)$$

The total training objective is the summation of the diffusion loss and the rendering loss.

$$\begin{aligned} \mathcal{L} &= \mathcal{L}_{diff} + \lambda_t \mathcal{L}_{rend}, \\ \mathcal{L}_{diff} &= \|\mathbf{L}_{\phi} - \mathbf{L}_0\|^2 + \|\epsilon_{\phi} - \epsilon\|^2, \\ \mathcal{L}_{rend} &= \sum_{\mathbf{r} \in \mathcal{R}} \|\hat{\mathbf{c}}(\mathbf{r}) - \mathbf{g}_{\mathbf{c}}(\mathbf{r})\|^2 + \text{CE}(\hat{\mathbf{p}}(\mathbf{r}), \mathbf{g}_{\mathbf{p}}(\mathbf{r})), \end{aligned} \quad (11)$$

where $\hat{\mathbf{c}}(\mathbf{r})$ and $\hat{\mathbf{p}}(\mathbf{r})$ are the rendered RGB image and part map from ray \mathbf{r} , and $\mathbf{g}_{\mathbf{c}}(\mathbf{r})$ and $\mathbf{g}_{\mathbf{p}}(\mathbf{r})$ are the corresponding ground truths; CE means the cross-entropy loss function. Since the predicted voxel field of the diffusion model is reasonable only with the time t close to zero, we attach a time-dependent weight λ_t to the rendering loss: $\lambda_t = -\log(t)$.

4 Experiments

4.1 Experimental Setup

Dataset We collect four categories of 3D objects from ShapeNet [5], including Chair, Table, Airplane and Car. Each category comprises 500 objects, with a split of 400 for training and 100 for testing purposes. Utilizing BlenderProc [6], we render 100 views of each object at a resolution of 800×800 resolution. With the posed images, we use the public code base [41] to generate neural voxel fields.

Table 1: Font sizes of headings. Table captions should always be positioned *above* the tables. Note the KID metrics are multiplied by 1000.

Method	Chair		Table		Airplane		Car	
	FID↓	KID↓	FID↓	KID↓	FID↓	KID↓	FID↓	KID↓
Part-NeRF	69.44	14.29	75.78	26.91	83.84	42.10	133.2	77.73
SSD-NeRF	49.15	8.56	-	-	-	-	89.09	45.95
DiffRF	43.92	7.25	56.28	22.61	53.33	19.85	88.33	26.65
Ours	27.70	5.19	44.27	21.74	36.01	21.10	62.27	29.66

Table 2: Ablation study of the latent diffusion on Chair/Airplane. "LD" denotes "latent diffusion".

Method	Chair		Airplane	
	FID ↓	KID ↓	FID ↓	KID ↓
with LD	27.70	5.19	36.01	21.10
without LD	47.19	8.08	57.65	22.05

Table 3: Ablation of part aware shape decoder on Chair/Airplane. "PASD" denotes "part-aware shape decoder".

Method	Chair		Airplane	
	FID ↓	KID ↓	FID ↓	KID ↓
with PASD	27.70	5.19	36.01	21.10
without PASD	29.18	5.35	38.23	22.05

Implementation Details The resolution of the voxel field is $96 \times 96 \times 96$, and the resolution of the latent code is $64 \times$ lower than the voxel field. We train the model for 100,000 iterations and we do not train the part-aware shape decoder for the first 20,000 iterations to warm up the latent 3D diffusion model. We set $K = 4$ and $D = 128$ for the part code. For each iteration, we sample 8192 rays to calculate the rendering loss. For the architecture of 3D UNet, we set the base channel to 96 and the channel multiplier is [1, 2, 4], resulting 144M parameters of the whole model.

Evaluation We report the Fréchet Inception Distance (FID) and Kernel Inception Distance (KID) to evaluate the quality of rendered images. We evaluate the two metrics at a resolution of 800×800 . In practice, we generate 200 objects and 10 views for each object to calculate metrics.

4.2 Shape Generation

Quantitative comparison against state of the art. In Tab. 1, we conduct a quantitative comparison between our proposed method and state-of-the-art approaches. Part-NeRF [42] employs multiple neural radiance fields to represent a single object, but the complex and redundant architecture increases the learning difficulty, ultimately yielding lower quality results. SSDNeRF [31] introduces a diffusion model for generating neural tri-plane fields. While the tri-plane representation is efficient, it lacks geometric detail compared to voxel representation. Additionally, our method employs a 3D UNet, which has superior feature extraction capabilities compared to the 2D UNet utilized in SSDNeRF, leading to

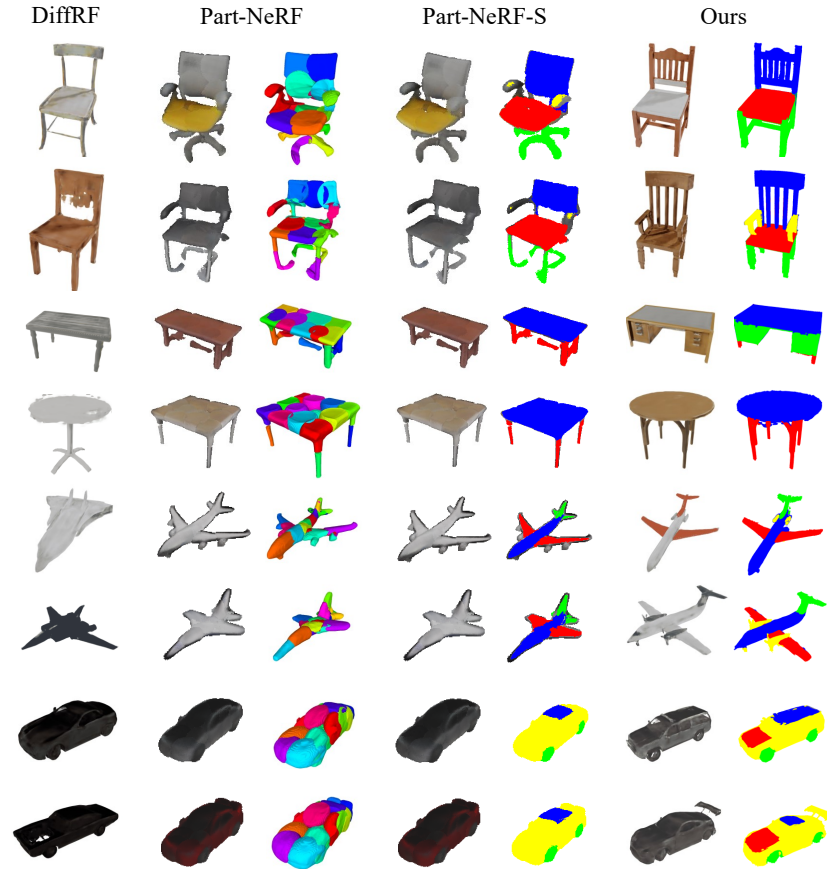


Fig. 3: Qualitative comparison against state of the art. Part-NeRF-S denotes adding the 2D part supervision to the original Part-NeRF.

enhanced performance. DiffRF [24] also utilizes the diffusion model in 3D space; however, it directly applies the 3D UNet to the voxel field. This implementation imposes significant computational demands, constraining the resolution of the voxel fields and leading to sub-optimal performances. We achieve the best FID metric on all classes, demonstrating the superiority of the proposed method.

Qualitative comparison against state of the art. As depicted in Fig. 3, we plot the visual generations of various state of the art methods. Leveraging the latent 3D diffusion model, we are able to generate high-resolution voxel fields, resulting in superior rendering quality. Similar to ours, Part-NeRF also produces part-aware rendering results. However, it employs an unsupervised approach that leads to the synthesis of meaningless structures. To ensure a fair comparison, we employ semantic part maps to supervise Part-NeRF, denoting this as

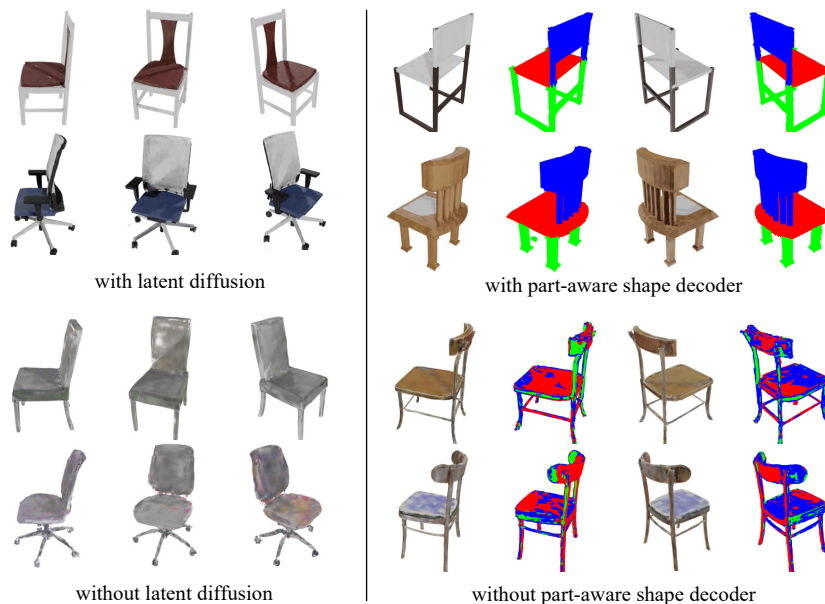


Fig. 4: Visual improvements of different components. left: importance of latent diffusion; right: importance of part-aware shape decoder.

Part-NeRF-S. Our approach still outperforms Part-NeRF-S in both texture and part quality. Both Quantitative and qualitative results indicate that the proposed method can generate accurate part-aware shapes and render high-quality images.

4.3 Ablation Studies

We ablate different components of the proposed method to show their importance. We conduct both quantitative and qualitative analyzes on the Chair data.

Importance of the latent 3D diffusion. In Fig. 2, we have demonstrated the importance of the 3D diffusion model. We further apply the diffusion process to the voxel field directly to observe the performance change. Due to the limitation of computational cost, we set the resolution of voxel fields to $32 \times 32 \times 32$. Tab. 2 reports the performance comparison. Without the latent diffusion, the FID and KID drop a lot, which shows the importance of latent diffusion. Moreover, we visualize the qualitative results of the two different settings in Fig. 4, and the results reveal that the latent 3D diffusion brings high-quality rendering details.

Importance of the part-aware shape decoder. The part-aware shape decoder incorporates the part code into the neural voxel field, generating the

structural shape with accurate rendering results. To demonstrate its importance, we replace it with two independent MLPs, rendering the color and part maps from the voxel field directly. Tab. 3 shows that the part-aware shape decoder can bring improvements in rendering quality. As depicted in Fig. 4, the part-aware shape decoder helps the model learn the accurate structural information.



Fig. 5: Visual improvements of the gradient skip.

Importance of the gradient skip. The gradient skip technique aims to reduce redundant gradient calculations and computational costs by jointly learning the latent 3D diffusion model and the part-aware shape decoder. In Fig. 5, we compare our method with the split training strategy, which does not utilize the gradient skip technique. It is evident from the comparison that the split training strategy lacking gradient skipping leads to the learning of a biased neural voxel field, consequently yielding inferior rendered images.

4.4 Shape Interpolation

Following the 2D diffusion model [40], we can utilize two different voxel fields to generate intermediate shapes with spherical linear interpolation [36]. As shown in Fig. 6, our model can achieve relatively smooth interpolation between the two shapes. In contrast, the model without the part-aware shape decoder generates unreasonable contents, which further indicates the effectiveness of the part-aware shape decoder. With the part-aware shape decoder, the generated intermediate shapes consistently maintain a precise structure, suggesting that the decoder effectively learns to decompose the neural voxel fields with guidance of the part code.

4.5 Single Image to Shape

Single image to shape can be seen as a conditional generation task. In practice, we use Swin-S [21] as the image feature extractor to process the single image,

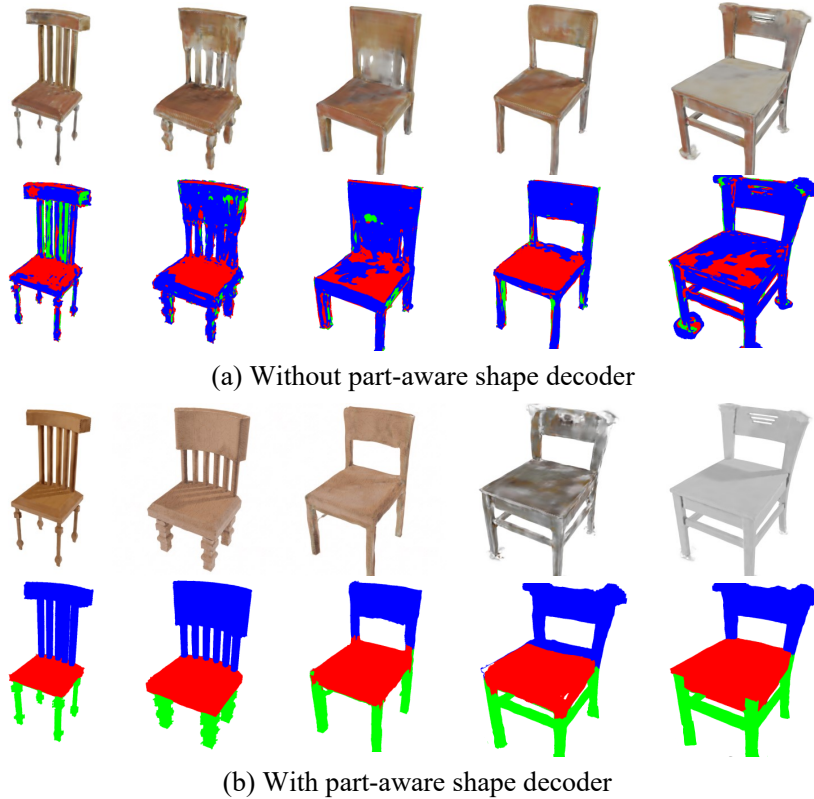


Fig. 6: Visualization of shape interpolation. The generated intermediate shapes also have an accurate part-aware structure.

and then concatenate the obtained features with the multi-scale features of the denoising UNet. As shown in Fig. 7, given a reference image as condition, our model can generate reasonable shapes with consistent geometry and accurate structure.

5 Conclusion

In this paper, we introduce a method for generating part-aware neural voxel fields using latent 3D diffusion models. The proposed method consists of a latent 3D diffusion model and a part-aware shape decoder. On one hand, the latent 3D diffusion model enhances the high-resolution of the neural voxel fields, thereby improving the geometric details and the quality of rendered images. On the other hand, the part-aware shape decoder integrates part codes into voxel fields

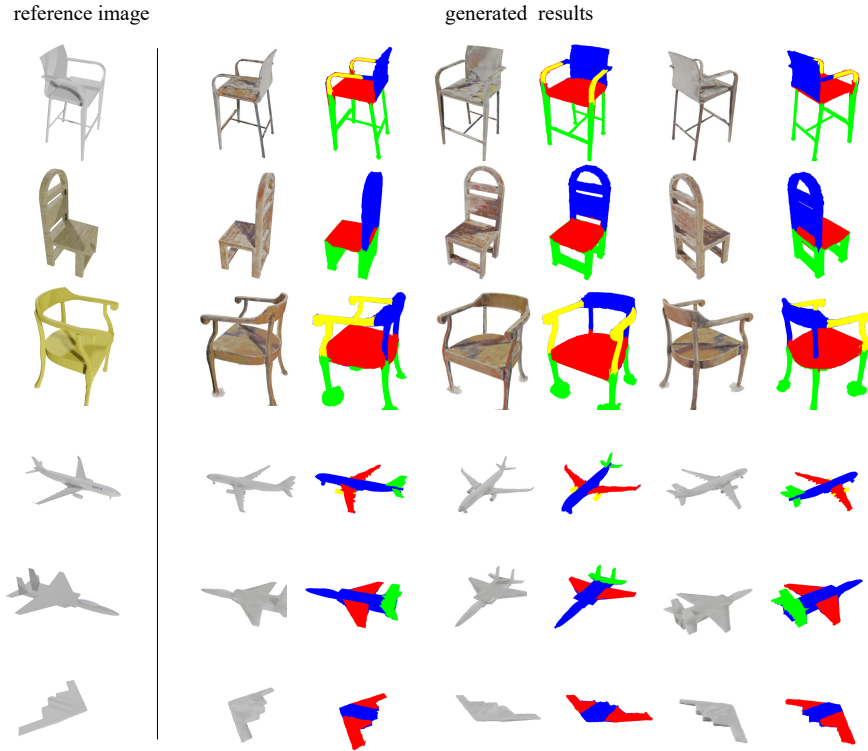


Fig. 7: Single image to shape generation. As depicted in the figure, the generated shape has a similar geometry as the reference image but with different textures, which indicates the model learns more geometry information from the reference image.

to generate part-aware shapes with high-quality rendered images. We evaluate the effectiveness of our method on four classes by comparing it against state-of-the-art diffusion-based approaches, demonstrating its efficacy in generating precise part-aware shapes.

6 Limitation and Future Work

The proposed method achieves precise part-aware generation and high-quality rendering outcomes. However, acquiring 2D semantic part maps for supervision may pose challenges due to the difficulty in collecting labeled part maps. With the emergence of semantic big models like [18], we anticipate a significant reduction in this collection cost. Our goal is to implement pseudo-label based part-aware generation in future work.

7 More Training Details

Additional Training Loss. The main loss of training the network comprises two parts: diffusion loss \mathcal{L}_{diff} and rendering loss \mathcal{L}_{rend} . Besides, we adopt two additional regularization loss functions. First, we conduct the total variation on the neural voxel fields to restrain the noise of generating:

$$\mathcal{L}_{tv} = \sum_{dim \in [D]} \sqrt{\Delta_x^2(\hat{\mathbf{V}}_0^f, dim) + \Delta_y^2(\hat{\mathbf{V}}_0^f, dim) + \Delta_z^2(\hat{\mathbf{V}}_0^f, dim)}, \quad (12)$$

where $\Delta_x^2(\hat{\mathbf{V}}_0^f, dim)$ denotes the squared difference between the value of dim -th channel in voxel: $v := (i; j; k)$ and the dim -th value in voxel $(i + 1; j; k)$, which can be extended to $\Delta_y^2(\hat{\mathbf{V}}_0^f, dim)$ and $\Delta_z^2(\hat{\mathbf{V}}_0^f, dim)$. Moreover, we constrain the value of part code \mathbf{z} via its L2 norm $\|\mathbf{z}\|_2$ attached with the weight 0.0001.

Sampling steps. Benefiting from fast sampling of the decoupled diffusion model, we can get satisfied results with only 30 steps. Tab. 4 reports the performance comparisons of different sampling steps for generating chairs.

Table 4: Performance comparisons of different sampling steps for generating chairs.

Step	10	20	30	40	50
FID↓	38.49	30.70	27.70	26.68	26.01
KID↓	7.25	6.15	5.19	5.08	5.01

8 More Visual Results

We depict more comparisons with the supervision version of Part-NeRF (Part-NeRF-S) in Fig. 8. As a result, our method can generate higher-quality outcomes with more accurate structures. More generated samples can be found in Fig. 9 and Fig. 10.

References

- Achlioptas, P., Diamanti, O., Mitliagkas, I., Guibas, L.: Learning representations and generative models for 3d point clouds. In: International conference on machine learning (2018)
- Bautista, M.A., Guo, P., Abnar, S., Talbott, W., Toshev, A., Chen, Z., Dinh, L., Zhai, S., Goh, H., Ulbricht, D., et al.: Gaudi: A neural architect for immersive 3d scene generation. Advances in Neural Information Processing Systems (2022)
- Chan, E.R., Lin, C.Z., Chan, M.A., Nagano, K., Pan, B., De Mello, S., Gallo, O., Guibas, L.J., Tremblay, J., Khamis, S., et al.: Efficient geometry-aware 3d generative adversarial networks. In: Proceedings of the IEEE/CVF Conference on Computer Vision and Pattern Recognition (2022)



Fig. 8: Visual comparisons to Part-NeRF-S.

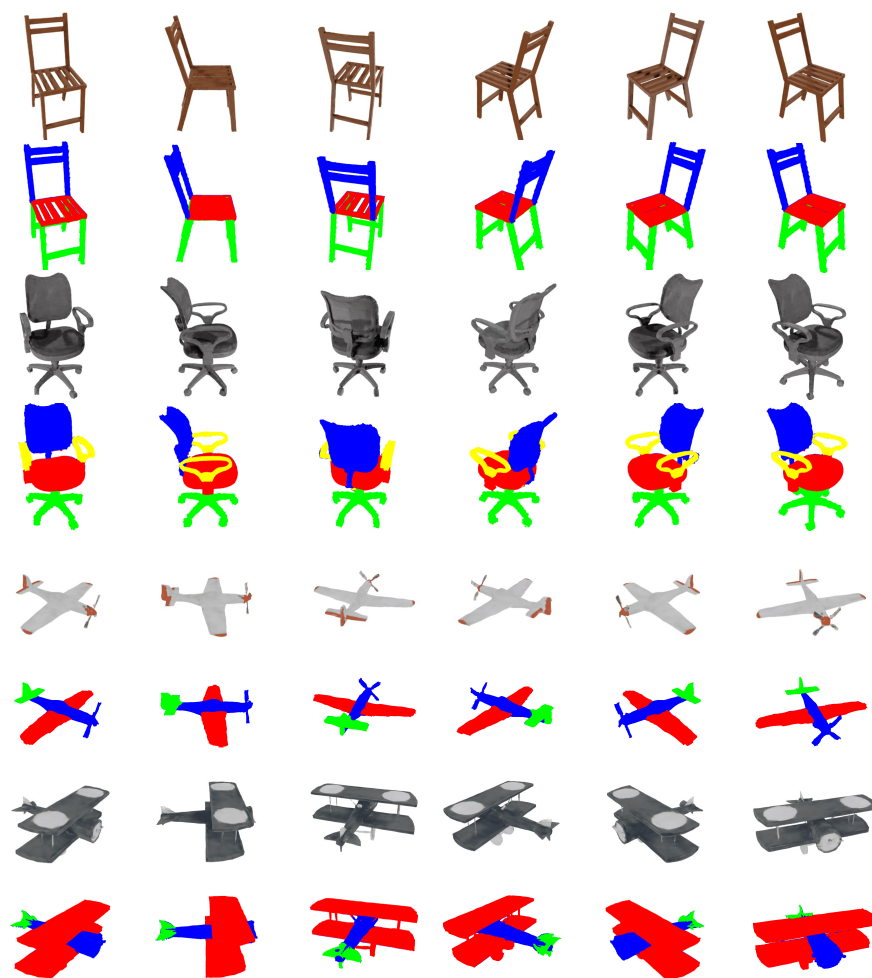


Fig. 9: Generated samples of chair and airplane.

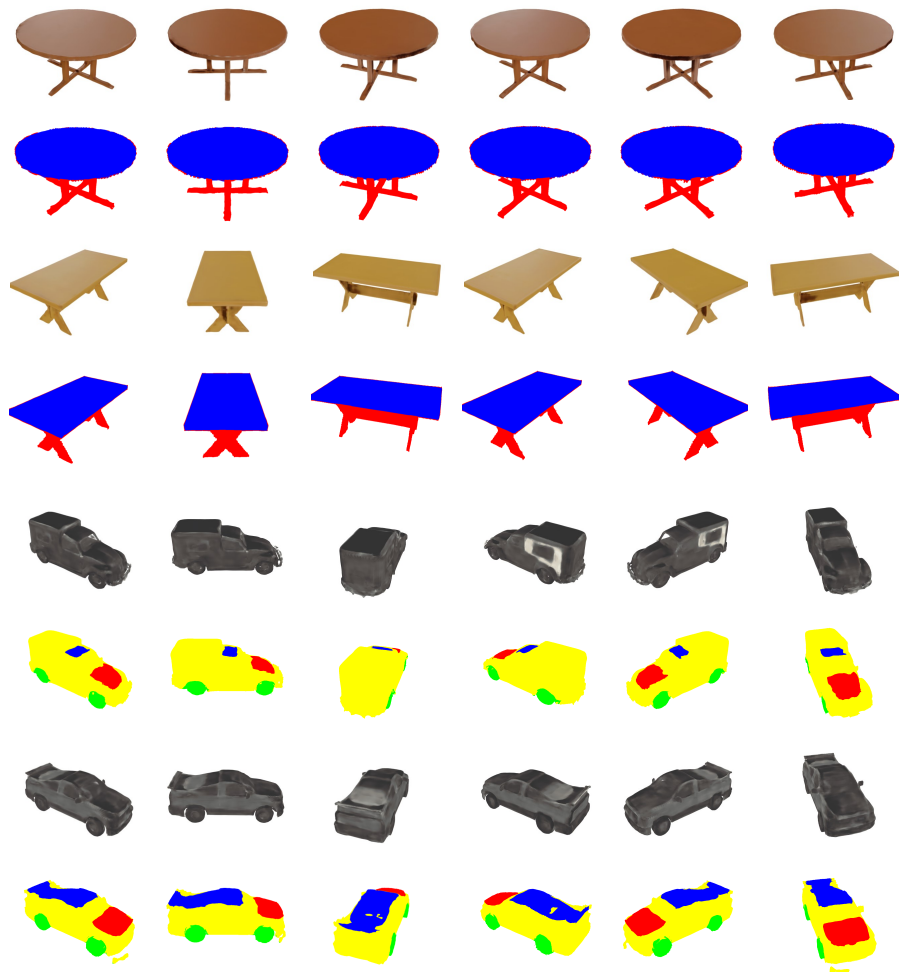


Fig. 10: Generated samples of table and car.

4. Chan, E.R., Monteiro, M., Kellnhofer, P., Wu, J., Wetzstein, G.: pi-gan: Periodic implicit generative adversarial networks for 3d-aware image synthesis. In: Proceedings of the IEEE/CVF conference on computer vision and pattern recognition (2021)
5. Chang, A.X., Funkhouser, T., Guibas, L., Hanrahan, P., Huang, Q., Li, Z., Savarese, S., Savva, M., Song, S., Su, H., et al.: Shapenet: An information-rich 3d model repository. arXiv preprint arXiv:1512.03012 (2015)
6. Denninger, M., Sundermeyer, M., Winkelbauer, D., Olefir, D., Hodan, T., Zidan, Y., Elbadrawy, M., Knauer, M., Katam, H., Lodhi, A.: Blenderproc: Reducing the reality gap with photorealistic rendering. In: International Conference on Robotics: Science and Systems, RSS 2020 (2020)
7. DeVries, T., Bautista, M.A., Srivastava, N., Taylor, G.W., Susskind, J.M.: Unconstrained scene generation with locally conditioned radiance fields. In: Proceedings of the IEEE/CVF International Conference on Computer Vision (2021)
8. Dhariwal, P., Nichol, A.: Diffusion models beat gans on image synthesis. *Advances in neural information processing systems* (2021)
9. Dupont, E., Kim, H., Eslami, S.M.A., Rezende, D.J., Rosenbaum, D.: From data to functa: Your data point is a function and you can treat it like one. In: International Conference on Machine Learning (2022)
10. Gao, J., Shen, T., Wang, Z., Chen, W., Yin, K., Li, D., Litany, O., Gojcic, Z., Fidler, S.: Get3d: A generative model of high quality 3d textured shapes learned from images. *Advances In Neural Information Processing Systems* (2022)
11. Goodfellow, I., Pouget-Abadie, J., Mirza, M., Xu, B., Warde-Farley, D., Ozair, S., Courville, A., Bengio, Y.: Generative adversarial nets. *Advances in neural information processing systems* (2014)
12. Gu, J., Liu, L., Wang, P., Theobalt, C.: Stylenerf: A style-based 3d aware generator for high-resolution image synthesis. In: The Tenth International Conference on Learning Representations (2022)
13. Hao, Z., Averbuch-Elor, H., Snavely, N., Belongie, S.: Dualsdf: Semantic shape manipulation using a two-level representation. In: Proceedings of the IEEE/CVF Conference on Computer Vision and Pattern Recognition (2020)
14. Henzler, P., Mitra, N.J., Ritschel, T.: Escaping plato’s cave: 3d shape from adversarial rendering. In: Proceedings of the IEEE/CVF International Conference on Computer Vision (2019)
15. Hertz, A., Perel, O., Giryas, R., Sorkine-Hornung, O., Cohen-Or, D.: Spaghetti: Editing implicit shapes through part aware generation. *ACM Transactions on Graphics (TOG)* (2022)
16. Ho, J., Jain, A., Abbeel, P.: Denoising diffusion probabilistic models. *Advances in neural information processing systems* (2020)
17. Huang, Y., Qin, Z., Liu, X., Xu, K.: Decoupled diffusion models with explicit transition probability. arXiv preprint arXiv:2306.13720 (2023)
18. Kirillov, A., Mintun, E., Ravi, N., Mao, H., Rolland, C., Gustafson, L., Xiao, T., Whitehead, S., Berg, A.C., Lo, W., Dollár, P., Girshick, R.B.: Segment anything. In: IEEE/CVF International Conference on Computer Vision (2023)
19. Li, R., Li, X., Hui, K.H., Fu, C.W.: Sp-gan: Sphere-guided 3d shape generation and manipulation. *ACM Transactions on Graphics (TOG)* (2021)
20. Liao, Y., Schwarz, K., Mescheder, L., Geiger, A.: Towards unsupervised learning of generative models for 3d controllable image synthesis. In: Proceedings of the IEEE/CVF conference on computer vision and pattern recognition (2020)

21. Liu, Z., Lin, Y., Cao, Y., Hu, H., Wei, Y., Zhang, Z., Lin, S., Guo, B.: Swin transformer: Hierarchical vision transformer using shifted windows. In: Proceedings of the IEEE/CVF international conference on computer vision (2021)
22. Long, X., Guo, Y.C., Lin, C., Liu, Y., Dou, Z., Liu, L., Ma, Y., Zhang, S.H., Habermann, M., Theobalt, C., et al.: Wonder3d: Single image to 3d using cross-domain diffusion. arXiv preprint arXiv:2310.15008 (2023)
23. Mildenhall, B., Srinivasan, P., Tancik, M., Barron, J., Ramamoorthi, R., Ng, R.: Nerf: Representing scenes as neural radiance fields for view synthesis. In: European conference on computer vision (2020)
24. Müller, N., Siddiqui, Y., Porzi, L., Bulo, S.R., Kotschieder, P., Nießner, M.: Diffrf: Rendering-guided 3d radiance field diffusion. In: Proceedings of the IEEE/CVF Conference on Computer Vision and Pattern Recognition (2023)
25. Nguyen-Phuoc, T., Li, C., Theis, L., Richardt, C., Yang, Y.L.: Hologan: Unsupervised learning of 3d representations from natural images. In: Proceedings of the IEEE/CVF International Conference on Computer Vision (2019)
26. Nguyen-Phuoc, T.H., Richardt, C., Mai, L., Yang, Y., Mitra, N.: Blockgan: Learning 3d object-aware scene representations from unlabelled images. Advances in neural information processing systems (2020)
27. Niemeyer, M., Geiger, A.: Giraffe: Representing scenes as compositional generative neural feature fields. In: Proceedings of the IEEE/CVF Conference on Computer Vision and Pattern Recognition (2021)
28. Petrov, D., Gadelha, M., Měch, R., Kalogerakis, E.: Anise: Assembly-based neural implicit surface reconstruction. IEEE Transactions on Visualization and Computer Graphics (2023)
29. Poole, B., Jain, A., Barron, J.T., Mildenhall, B.: Dreamfusion: Text-to-3d using 2d diffusion. In: The Eleventh International Conference on Learning Representations (2023)
30. Qian, G., Mai, J., Hamdi, A., Ren, J., Siarohin, A., Li, B., Lee, H.Y., Skorokhodov, I., Wonka, P., Tulyakov, S., et al.: Magic123: One image to high-quality 3d object generation using both 2d and 3d diffusion priors. arXiv preprint arXiv:2306.17843 (2023)
31. Ranade, S., Lassner, C., Li, K., Häne, C., Chen, S., Bazin, J., Bouaziz, S.: Ssdnerf: Semantic soft decomposition of neural radiance fields. CoRR (2022)
32. Rombach, R., Blattmann, A., Lorenz, D., Esser, P., Ommer, B.: High-resolution image synthesis with latent diffusion models. In: Proceedings of the IEEE/CVF conference on computer vision and pattern recognition (2022)
33. Schwarz, K., Liao, Y., Niemeyer, M., Geiger, A.: Graf: Generative radiance fields for 3d-aware image synthesis. Advances in Neural Information Processing Systems (2020)
34. Schwarz, K., Sauer, A., Niemeyer, M., Liao, Y., Geiger, A.: Voxgraf: Fast 3d-aware image synthesis with sparse voxel grids. Advances in Neural Information Processing Systems (2022)
35. Sharma, G., Liu, D., Maji, S., Kalogerakis, E., Chaudhuri, S., Měch, R.: Parsenet: A parametric surface fitting network for 3d point clouds. In: European conference on computer vision (2020)
36. Shoemake, K.: Animating rotation with quaternion curves. In: Proceedings of the 12th annual conference on Computer graphics and interactive techniques (1985)
37. Siddiqui, Y., Thies, J., Ma, F., Shan, Q., Nießner, M., Dai, A.: Texturify: Generating textures on 3d shape surfaces. In: European Conference on Computer Vision (2022)

38. Skorokhodov, I., Tulyakov, S., Wang, Y., Wonka, P.: Epigraf: Rethinking training of 3d gans. *Advances in Neural Information Processing Systems* (2022)
39. Sohl-Dickstein, J., Weiss, E., Maheswaranathan, N., Ganguli, S.: Deep unsupervised learning using nonequilibrium thermodynamics. In: *International conference on machine learning* (2015)
40. Song, J., Meng, C., Ermon, S.: Denoising diffusion implicit models. In: *ICLR* (2021)
41. Sun, C., Sun, M., Chen, H.T.: Direct voxel grid optimization: Super-fast convergence for radiance fields reconstruction. In: *Proceedings of the IEEE/CVF Conference on Computer Vision and Pattern Recognition* (2022)
42. Tertikas, K., Despoina, P., Pan, B., Park, J.J., Uy, M.A., Emiris, I., Avrithis, Y., Guibas, L.: Partnerf: Generating part-aware editable 3d shapes without 3d supervision. In: *Proceedings of the IEEE/CVF conference on computer vision and pattern recognition* (2023)
43. Vaswani, A., Shazeer, N., Parmar, N., Uszkoreit, J., Jones, L., Gomez, A.N., Kaiser, Ł., Polosukhin, I.: Attention is all you need. *Advances in neural information processing systems* (2017)
44. Wu, J., Zhang, C., Xue, T., Freeman, B., Tenenbaum, J.: Learning a probabilistic latent space of object shapes via 3d generative-adversarial modeling. *Advances in neural information processing systems* (2016)
45. Wu, R., Zhuang, Y., Xu, K., Zhang, H., Chen, B.: Pq-net: A generative part seq2seq network for 3d shapes. In: *Proceedings of the IEEE/CVF Conference on Computer Vision and Pattern Recognition* (2020)
46. Zhou, P., Xie, L., Ni, B., Tian, Q.: CIPS-3D: A 3d-aware generator of gans based on conditionally-independent pixel synthesis. *CoRR* (2021)
47. Zhou, Z., Tulsiani, S.: Sparsefusion: Distilling view-conditioned diffusion for 3d reconstruction. In: *Proceedings of the IEEE/CVF Conference on Computer Vision and Pattern Recognition* (2023)